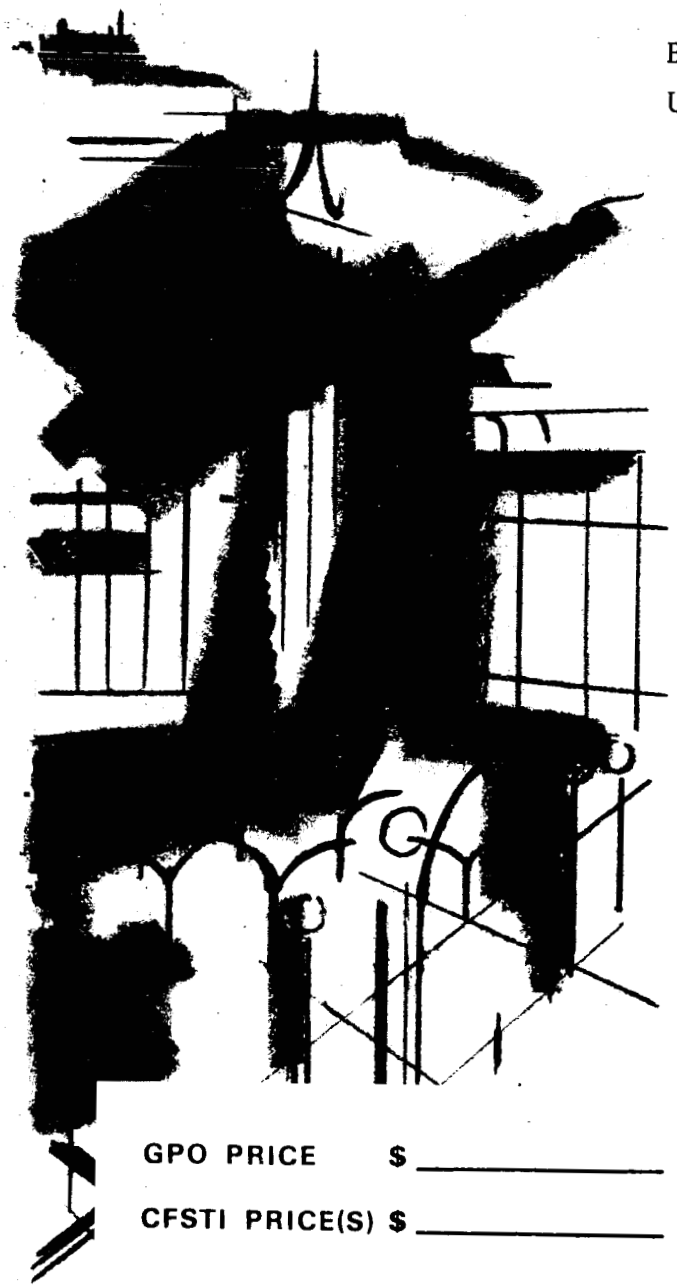

BREAKDOWN OF A LIQUID FILAMENT INTO DROPS UNDER THE ACTION OF ACOUSTIC DISTURBANCES

By

Robert Henry Wickemeyer

A. K. Oppenheim
Faculty Investigator

Technical Note No. 1-67
NASA Grant NsG-702
Report No. As-67-6

June 1967

COLLEGE OF ENGINEERING
UNIVERSITY OF CALIFORNIA, Berkeley

OFFICE OF RESEARCH SERVICES
University of California
Berkeley, California 94720

BREAKDOWN OF A LIQUID FILAMENT INTO DROPS UNDER THE ACTION OF ACOUSTIC DISTURBANCES

By
Robert Henry Wickemeyer
and
A. K. Oppenheim

Technical Note No. 1-67
NASA Grant NsG-702
Report No. AS-67-6

June 1967

ABSTRACT

For the purpose of producing small uniform drops for spray combustion experimentation, the theoretical and experimental aspects of the breakdown of a liquid filament into drops under the action of acoustic disturbances are studied. The theory expands the Rayleigh criterion for capillary instability of jets by introducing additional terms to account for aerodynamic forces and fluid viscosity. Experimental results indicate that there exists, at each flow rate, a spread of frequencies capable of producing uniform drops, rather than unique frequency as predicted by the theory and that, for Reynolds numbers in excess of 600, the size of drops is independent of the filament velocity.

TABLE OF CONTENTS

ACKNOWLEDGMENT

The experimental work reported here was initiated by Dr. S. Wojcicki who was primarily responsible for the design of the spray-head, photography of the break-up of the liquid filament, and the introduction of the Ohnesorge number as an important non-dimensional correlating parameter for experimental results. Thus the author wishes to take this opportunity to express his appreciation for the help he received from Dr. Wojcicki. He would also like to express his thanks to Messrs. Val Vesninsky, Walter Giba and Ken Hom for their assistance in the construction of the experimental apparatus.

NOMENCLATURE

a	initial radius of the jet
d	initial diameter of the jet
f	frequency of jet varicosity
ℓ	wave length of the varicosity of the jet, see Fig. 5
p	pressure
q_σ	pressure variation due to the surface tension of the varicose jet
r	radial direction of the jet
t	time
u	component of velocity in x direction
v	component of velocity in r direction
x	downstream direction of the jet
C_p	pressure coefficient
I_J, J_J, K_J	Bessel functions
L	length of tube generating liquid jet
P	non-dimensional pressure, see Eq. (12)
Q_a	non-dimensional pressure variation due to aerodynamic forces, see Eq. (14h)
Q_σ	non-dimensional pressure variation due to surface tension, see Eq. (14g)
R	non-dimensional radial direction
R_1, R_2	jet radii of curvature
Re	Reynolds number based on fluid properties and initial jet diameter
Re_a	Reynolds number based on initial jet radius
St	Strouhal number, see Eq. (35)

T	non-dimensional time
U	non-dimensional x velocity component
U_s	initial u velocity of the jet
V	non-dimensional r velocity component, see Eq. (12)
We_a	Weber number based on fluid properties and initial jet radius
X	non-dimensional downstream direction
Z	Ohnesorge number
α	wave parameter
η	amplification factor for streamline or surface displacement
λ	deflection of a streamline at mean radius r
λ^*	amplitude factor for streamline or surface displacement
μ	viscosity coefficient
ρ	density
σ	surface tension of the liquid
φ	dimensional velocity potential
Γ	non-dimensional parameter of the form $\frac{\mu c}{\sigma}$ where c is the speed of sound in the fluid
Δ, Δ_1	differential operators defined by Eq. (13)
H	non-dimensional amplification factor
Λ	non-dimensional streamline deflection, see Eq. (12)
$\mathfrak{G}$	distribution coefficient of Eq. (23)
Φ	velocity potential

Superscript

$-$	value of the parameter taken at the surface of the jet
$*$	amplitude component of the parameter

INTRODUCTION

Analysis of the generation of pressure waves caused by combustion or detonations is tractable when both fuel and oxidizing components are in the gaseous phase. When the fuel is in a condensed phase, the problem is much more complex, however, a considerable simplification is attained if fuel particles are assumed to be of a uniform size. In fact a solution of the problem of the generation of pressure waves in particle-fueled combustion systems has been obtained at this laboratory.[1] The generation of such a liquid fuel-gaseous oxidizer environment became, therefore, of practical significance, and the study of practical means for this purpose is reported here.

It has been found that systems containing drops of less than 15 microns in size behave similarly to a gaseous mixture.[2] In practical combustion chambers, however, drops may have mean sizes of a 1000 microns. Hence, in order to investigate the entire spectrum of spray combustion, the generation of uniform drops in the range of 15 to 1000 microns is of particular importance.

So as to cover the entire range of drop size and flow rate imposed by the combustion experiment, acoustic as well as ultrasonic devices are required. The operation of both devices may be based on the instability of a liquid filament, and thus the study of this problem constituted the major effort of the investigation reported here. An expansion on the classic theory of capillary instability has been established to include the effects of viscosity and jet velocity and its results have been checked by experiments in the acoustic range.

CAPILLARY INSTABILITY

Introduction:

Various techniques[3-14] for generation of uniform drops have been reported in the literature. Figure 1 summarizes some of the possible methods for mechanical drop generation. For the purposes of the combustion experiment only methods c and d were considered applicable. Figure 2a shows droplets formed by method c, and Fig. 2b by method d.

All of these methods consist of subjecting a liquid filament to a periodic force. It is shown below that when this periodic force is at critical frequencies, the stream is divided up into droplets of equal size. In order to obtain uniform size drops, one has to avoid the generation of satellites as illustrated by Fig. 3a. Only when they reach a very small size, as in Fig. 3b, can the satellites be absorbed by the larger drops. Furthermore, all of the above methods of generating uniform droplets exhibit the same dependence of frequency on flow rate. Thus a theory proven for one method of imparting periodic mechanical forces on liquid filaments should be applicable to all other methods. The data presented in this report was generated by means of method c and d of Fig. 1. Method d was selected as the most practical one for further studies in two-phase combustion research. A more detailed drawing of a spray head utilizing this technique is presented on Fig. 4.

The analysis of the problem of capillary instability of a varicose filament was first performed by Lord Rayleigh in 1877 as a surface tension exercise. This led to the establishment of the so-called Rayleigh criterion to the effect that "the maximum instability occurs when the wave length of the disturbance is 4.51 times the initial jet diameter".[16, 17] Rayleigh's analysis was based on an inviscid fluid and his results were independent of the velocity of the jet. Later Weber [18] and more recently Chandrasekhar [19] have reworked the problem including the effects of viscosity and body forces such as those associated with hydromagnetic effects. The approach of Chandrasekhar is mathematically quite sophisticated while Weber's analysis, being more elementary in this respect, lends itself to a more direct physical insight into the problem. The theory described here is, therefore, inspired primarily on Weber's work.

Formulation of the Problem:

For a varicose filament as illustrated in Fig. 5 with small surface deflections and small velocity perturbations it can be assumed that local acceleration terms ($\frac{\partial u}{\partial t}$ or $\frac{\partial v}{\partial t}$) are predominant over convective acceleration

terms ($u \frac{\partial u}{\partial x}$ or $v \frac{\partial v}{\partial y}$). Thus, neglecting gravity, the flow in the filament can be described by Navier-Stokes equations in cylindrical coordinates:

$$\rho \frac{\partial u}{\partial t} = - \frac{\partial p}{\partial x} + \mu \left[\frac{\partial^2 u}{\partial x^2} + \frac{\partial^2 u}{\partial r^2} + \frac{1}{r} \frac{\partial u}{\partial r} \right], \tag{1}$$

$$\rho \frac{\partial v}{\partial t} = - \frac{\partial p}{\partial r} + \mu \left[\frac{\partial^2 v}{\partial x^2} + \frac{\partial^2 v}{\partial r^2} + \frac{1}{r} \frac{\partial v}{\partial r} - \frac{v}{r^2} \right]. \tag{2}$$

As a consequence of neglecting the convective acceleration, the kinematic relation between the radial velocity and the displacement of the surface, $\bar{\lambda}$, from its initial radius, a, is simply:

$$v_{r=a} = \frac{\partial \bar{\lambda}}{\partial t} . \tag{3}$$

The incompressible continuity equation for the liquid filament is

$$\frac{\partial u}{\partial x} + \frac{\partial v}{\partial r} + \frac{v}{r} = 0 . \tag{4}$$

The boundary conditions for this problem are as follows. First, the shear stress in the axial direction vanishes at the surface, hence:

$$\left(\frac{\partial u}{\partial r} + \frac{\partial v}{\partial x} \right)_{r=a} = 0 \tag{5}$$

and second, the normal component of the viscous stress at the surface of the varicose filament is balanced by surface tension and the aerodynamic pressure of the external gas:

$$\left(p - 2\mu \frac{\partial v}{\partial r} \right)_{r=a} = q_\sigma + q_a . \tag{6}$$

With reference to Fig. 5, the pressure component corresponding to the dis-

placement of the surface from its initial radius, a, is

$$q_\sigma = \sigma\left(\frac{1}{R_1} + \frac{1}{R_2} - \frac{1}{a}\right) ,$$

where R_1, the radius of curvature of the jet surface in the Xr plane, and R_2, the corresponding radius in a cross-sectional plane, are, in first order approximation, expressed as:

$$\frac{1}{R_1} \cong - \frac{\partial^2 \bar{r}}{\partial x^2} ,$$

$$\frac{1}{R_2} \cong \frac{1}{\bar{r}} ,$$

with $\bar{r} = a + \bar{\lambda}$.

Then

$$q_\sigma = \sigma\left(\frac{1}{a^2} + \frac{\partial^2}{\partial x^2}\right)\bar{\lambda} . \tag{7}$$

Since the surface deflection of the filament is small, small perturbation theory may be applied to evaluate the aerodynamic pressure, q_a. For axisymmetric flow this is then:

$$q_a = \frac{1}{2}\rho_{air} U_s^2 C_p = -\frac{1}{2}\rho_{air} U_s^2 \left[\frac{2}{U_s}\frac{\partial \varphi}{\partial x} - \frac{1}{U_s^2}\left(\frac{\partial \varphi}{\partial r}\right)^2\right], \tag{8}$$

where φ is the velocity potential of the external gas flow, which is given by

$$m^2 \frac{\partial^2 \varphi}{\partial x^2} + \frac{\partial^2 \varphi}{\partial r^2} + \frac{1}{r}\frac{\partial \varphi}{\partial r} = 0 , \tag{9}$$

with $m^2 \equiv 1 - M_\infty^2$ and where M_∞ is the free stream Mach number of the gas with respect to the liquid filament.

It is reasonable to assume [18] that the deviation of any given streamline in the liquid from its mean radius, r, can be expressed as:

$$\lambda = \lambda^* e^{\eta t} \cos 2\pi \frac{x}{\ell} , \tag{10}$$

or in terms of the wave parameter defined as

$$\alpha \equiv 2\pi \frac{a}{\ell} , \tag{10a}$$

$$\lambda = \lambda^* e^{\eta t} \cos \alpha \frac{x}{a} , \tag{10b}$$

where λ^* is a function of r, and η is a function of α.

Since the stream breaks up uniformly when $\frac{\partial \bar{\lambda}}{\partial \ell} = 0$ at $x=\ell$ and $\bar{\lambda} = -a$, it follows from Eq. (10b) that

$$\frac{\partial \bar{\lambda}}{\partial \ell}\Big|_{x=\ell, \bar{\lambda}=-a} = \frac{\partial \bar{\lambda}}{\partial \alpha} \cdot \frac{\partial \alpha}{\partial \ell}\Big|_{x=\ell, \bar{\lambda}=-a} = 0$$

and, since at $x=\ell$, $\sin \alpha \frac{x}{a} = 0$,

$$-\left(\bar{\lambda}^* e^{\eta t} (\cos \alpha \frac{x}{a}) \frac{\partial \eta}{\partial \alpha}\right) \frac{\alpha^2}{a}\Big|_{x=\ell, \bar{\lambda}=-a} = 0$$

which, for non-trivial solutions, is satisfied if, and only if,

$$\frac{\partial \eta}{\partial \alpha} = 0 . \tag{11}$$

The purpose of the analysis is, therefore, to determine the circumstances under which the condition of Eq. (11) is fulfilled. This is obtained by finding the relationship between the amplification factor, η, and the wave parameter, α, and from evaluating the coordinates at $\eta = \eta_{max}$.

Non-Dimensional Formulation:

The problem is reformulated first in terms of the following non-

dimensionalized parameters:

$$\left.\begin{aligned} &\Lambda = \frac{\lambda}{a}\ , \quad X = \frac{x}{\ell}\ , \quad R = \frac{r}{a}\ , \quad U = \frac{u}{U_s} \\ &V = \frac{v\ell}{U_s a}\ , \quad P = \frac{p}{\rho U_s^2}\ , \quad Q_\sigma = \frac{q_\sigma a}{\sigma}\ , \quad Q_a = \frac{q_a a}{\sigma} \\ &Re_a = \frac{\rho U_s a}{\mu}\ , \quad We_a = \frac{\rho U_s^2 a}{\sigma}\ , \quad T = \frac{t U_s}{\ell} \\ &H = \frac{\eta \ell}{U_s}\ , \quad \alpha = 2\pi \frac{a}{\ell}\ , \quad \Phi = \frac{\varphi}{U_s a}\ . \end{aligned}\right\} \tag{12}$$

In addition, it is also convenient to introduce the differential operators Δ and Δ_1 which are defined as:

$$\begin{aligned} \Delta &\equiv \frac{\alpha^2}{(2\pi)^2}\frac{\partial^2}{\partial X^2} + \frac{\partial^2}{\partial R^2} + \frac{1}{R}\frac{\partial}{\partial R}\ , \\ \Delta_1 &\equiv \frac{\alpha^2}{(2\pi)^2}\frac{\partial^2}{\partial X^2} + \frac{\partial^2}{\partial R^2} + \frac{1}{R}\frac{\partial}{\partial R} - \frac{1}{R^2}\ . \end{aligned} \tag{13}$$

The basic Eqs. (1) - (10) then become

$$\frac{\partial U}{\partial T} = -\frac{\partial P}{\partial X} + \frac{2\pi}{\alpha Re_a}\Delta U\ , \tag{14a}$$

$$\frac{\partial V}{\partial T} = -\frac{(2\pi)^2}{\alpha^2}\frac{\partial P}{\partial R} + \frac{2\pi}{\alpha Re_a}\Delta_1 V\ , \tag{14b}$$

$$\frac{\partial \Lambda}{\partial T} = V\ , \tag{14c}$$

$$\frac{\partial U}{\partial X} + \frac{\partial V}{\partial R} + \frac{V}{R} = 0\ , \tag{14d}$$

With boundary conditions:

$$\left(\frac{\partial U}{\partial R} + \frac{\alpha^2}{(2\pi)^2}\frac{\partial V}{\partial X}\right)_{R=1} = 0\ , \tag{14e}$$

$$\left(We_a P - \frac{\alpha}{\pi}\frac{We_a}{Re_a}\frac{\partial V}{\partial R}\right)_{R=1} = Q_\sigma + Q_a\ , \tag{14f}$$

where

$$Q_\sigma = -\left(1 + \frac{\alpha^2}{(2\pi)^2}\frac{\partial^2}{\partial X^2}\right)\bar{\Lambda}\,, \tag{14g}$$

$$Q_a = -\frac{We_a}{2}\left(\frac{\rho_{air}}{\rho}\right)\left[\frac{\alpha}{\pi}\frac{\partial \bar{\Phi}}{\partial X} + \left(\frac{\partial \bar{\Phi}}{\partial R}\right)^2\right], \tag{14h}$$

$$m^2\frac{\alpha^2}{(2\pi)^2}\frac{\partial^2\bar{\Phi}}{\partial X^2} + \frac{\partial^2\bar{\Phi}}{\partial R^2} + \frac{1}{R}\frac{\partial \bar{\Phi}}{\partial R}\,, \tag{14i}$$

and

$$\Lambda = \Lambda^* e^{\mathbf{H}T}\cos 2\pi X\,. \tag{14j}$$

General Solution:

The Navier-Stokes equations, Eq. (14a) and (14b) subject to constraints Eq. (14c) and (14d), can be used to find expressions for P and $\frac{\partial V}{\partial R}$ which appear in the second boundary condition, Eq. (14f). This is begun by differentiating Eq. (14a) with respect to X, differentiating Eq. (14b) with respect to R, multiplying Eq. (14b) by $\frac{1}{R}$, and adding the results to yield

$$\frac{\partial}{\partial T}\left(\frac{\partial U}{\partial X} + \frac{\partial V}{\partial R} + \frac{V}{R}\right) = -\left(\frac{\partial^2 P}{\partial X^2} + \frac{(2\pi)^2}{\alpha^2}\frac{\partial^2 P}{\partial R^2} + \frac{(2\pi)^2}{\alpha^2 R}\frac{\partial P}{\partial R}\right)$$
$$+ \frac{2\pi}{\alpha Re_a}\left(\frac{\partial}{\partial X}\Delta U + \frac{\partial}{\partial R}\Delta_1 V + \frac{1}{R}\Delta_1 V\right).$$

By continuity and the definition of the operators Δ and Δ_1 the above reduces to:

$$\Delta P = 0\,. \tag{15}$$

Applying the operator Δ_1 to Eq. (14b) and using Eq. (15) leads to:

$$\frac{\partial}{\partial T}\Delta_1 V = \frac{2\pi}{\alpha Re_a}\Delta_1^2 V\,. \tag{16}$$

Substituting Eq. (14c) to eliminate V gives:

$$\frac{\partial}{\partial T}\Delta_1\left(\frac{2\Pi}{Re_a\alpha}\Delta_1-\frac{\partial}{\partial T}\right)\Lambda=0\ . \tag{17}$$

Eq. (17) can be satisfied if

$$\frac{\partial}{\partial T}\Delta_1\Lambda_1=0\ ,$$

or with Eq. (14j)

$$\Delta_1\frac{\partial}{\partial T}\Lambda_1=\Delta_1\mathbf{H}\Lambda_1=0\ .$$

Since the operator Δ_1 only contains derivatives with respect to X and R, while $\mathbf{H}$ is only a function of α, this becomes

$$\Delta_1\Lambda_1=0\ . \tag{17a}$$

Eq. (17) is also satisfied by

$$\left(\Delta_1-\frac{\alpha Re_a}{2\Pi}\frac{\partial}{\partial T}\right)\Lambda_2=0\ . \tag{17b}$$

Eqs. (17a, b) can be looked upon as the particular solutions of Eq. (17) while its general solution is

$$\Lambda=\Lambda_1+\Lambda_2 \tag{17c}$$

or, according to Eq. (14c)

$$V=\frac{\partial\Lambda_1}{\partial T}+\frac{\partial\Lambda_2}{\partial T}\ .$$

Substituting the above into Eq. (14b) leads to:

$$P=-\frac{\alpha^2}{(2\Pi)^2}\frac{\partial^2}{\partial T^2}\int\Lambda_1\,dR\ . \tag{18}$$

Eqs. (14c) and (18) can be substituted into the boundary condition, Eq. (14f), once equations for Λ_1 and Λ_2 are found. Such expressions can be obtained by the use of Eq. (14j) with Eqs. (17a, b), leading to:

$$\left[-\alpha^2 + \frac{\partial^2}{\partial R^2} + \frac{1}{R}\frac{\partial}{\partial R} - \frac{1}{R^2}\right]\Lambda_1^* = 0 , \tag{19a}$$

and

$$\left[-\alpha^2 - \frac{\alpha H}{2\Pi} Re_a + \frac{\partial^2}{\partial R^2} + \frac{1}{R}\frac{\partial}{\partial R} - \frac{1}{R^2}\right]\Lambda_2^* = 0 . \tag{19b}$$

The above equations become identical in form if one introduces in Eq. (19b)

$$\alpha_1^2 \equiv \alpha^2 + \frac{\alpha H}{2\Pi} Re_a . \tag{20}$$

Their solutions are then Bessel functions with arguments αR and $\alpha_1 R$ respectively, namely:

$$\begin{aligned} \Lambda_1^* &= (1-\sigma)\bar{\Lambda}^* \frac{F_1(\alpha R)}{F_1(\alpha)} , \\ \Lambda_2^* &= \sigma \bar{\Lambda}^* \frac{F_1(\alpha_1 R)}{F_1(\alpha_1)} , \end{aligned} \tag{21}$$

where

$$F_1(\alpha R) \equiv -i J_1(i\alpha R) .$$

The distribution coefficient, σ, has been introduced to satisfy the condition of Eq. (17c), $\bar{\Lambda} = \Lambda_1 + \Lambda_2$. This coefficient is, in turn, determined by differentiating the first boundary condition, Eq. (14e), with respect to X and eliminating U with the continuity equation, Eq. (14d), yielding

$$\left[\Delta_1 - \frac{\alpha^2}{2\Pi^2}\frac{\partial^2}{\partial X^2}\right]\bar{\Lambda} = 0 .$$

Taking into account Eqs. (17a,b), this becomes

$$Re_a \frac{\alpha}{2\pi} \frac{\partial \Lambda_2}{\partial T} - \frac{\alpha^2}{2\pi^2} \frac{\partial^2}{\partial X^2} (\bar{\Lambda}_1 + \bar{\Lambda}_2) = 0 . \tag{22}$$

Inserting Eqs. (21) into (22) the distribution coefficient is found to be

$$G = - \frac{4\pi\alpha}{Re_a H} . \tag{23}$$

With Eqs. (21) and (23), the integral and double derivative terms of Eq. (14f) may now be expressed as follows:

$$\frac{\partial^2}{\partial T^2} \int \Lambda_1 dR = \frac{\partial^2}{\partial T^2} \left[\frac{(1-G)\bar{\Lambda}^*}{\alpha F_1(\alpha)} e^{HT} \cos 2\pi X \int F_1(\alpha R) d(\alpha R) \right]$$

$$= H^2 \left[\frac{(1-G)}{\alpha} \frac{F_0(\alpha R)}{F_1(\alpha)} \right] \bar{\Lambda} , \tag{24a}$$

and

$$\frac{\partial^2}{\partial R \partial T} (\bar{\Lambda}_1 + \bar{\Lambda}_2) = H e^{HT} \cos 2\pi X \frac{\partial}{\partial R} (\Lambda_1^* + \Lambda_2^*)$$

$$= H \left[(1-G)\alpha \frac{F_1'(\alpha R)}{F_1(\alpha)} + G\alpha_1 \frac{F_1'(\alpha R)}{F_1(\alpha)} \right] \bar{\Lambda} . \tag{24b}$$

Surface Tension:

An expression for the pressure component on the surface of the filament due to surface tension is obtained by substituting the surface equation, Eq. (14j), into Eq. (14g), yielding

$$Q_\sigma = - \left[1 - \alpha^2 \right] \bar{\Lambda} . \tag{25}$$

Aerodynamic Pressure:

To obtain an expression for the aerodynamic pressure component, Eq. (14i) must be solved for the velocity potential $\bar{\Phi}$.

$$\frac{m^2\alpha^2}{(2\pi)^2}\frac{\partial^2\bar{\Phi}}{\partial X^2} + \frac{\partial^2\bar{\Phi}}{\partial R^2} + \frac{1}{R}\frac{\partial\bar{\Phi}}{\partial R} = 0 .$$

By separation of variables

$$\bar{\Phi} = E(X)\cdot G(R) , \tag{26}$$

whence

$$E(X) = A_1 \cos kX + A_2 \sin kX ,$$

$$G(R) = B_1 I_o\left(mk\frac{\alpha}{2\pi}R\right) + B_2 K_o\left(mk\frac{\alpha}{2\pi}R\right),$$

where I_o and K_o are modified Bessel functions and A_1, A_2, B_1, B_2 and k are constants. Since at infinity, $\bar{\Phi}$ must be finite, $B_1 \equiv 0$ because as $R\to\infty$, $I_o\left(mk\frac{\alpha}{2\pi}R\right)\to\infty$. The tangent flow boundary condition for axisymmetric flow at a surface is

$$\lim_{r\to\bar{r}} r\frac{\partial\varphi}{\partial r} = r U_s \frac{\partial\bar{r}}{\partial x} ,$$

or in non-dimensional form

$$\lim_{R\to\bar{R}} R\frac{\partial\bar{\Phi}}{\partial R} = R\frac{\alpha}{2\pi}\frac{\partial\bar{R}}{\partial X} , \tag{27}$$

where $$\bar{R} = 1 + \bar{\Lambda}^* e^{HT}\cos 2\pi X = 1 + \bar{\Lambda} . \tag{28}$$

By virtue of Eqs. (26) and (28), $\frac{\partial \Phi}{\partial R}$ and $\frac{\partial \bar{R}}{\partial X}$ are expressed as follows:

$$\frac{\partial \Phi}{\partial R} = - \left[A_1 \cos kX + A_2 \sin kX\right] B_2 m k \frac{\alpha}{2\pi} K_1\left(m k \frac{\alpha}{2\pi} R\right),$$

$$\frac{\partial \bar{R}}{\partial X} = - 2\pi \bar{\Lambda}^* e^{HT} \sin 2\pi X .$$

Noting that $\bar{\Lambda}^* \ll 1$, Eq. (27) yields then:

$$A_1 = 0 , \quad A_2 B_2 = \frac{\bar{\Lambda}^* e^{HT}}{m K_1(m\alpha)} , \quad k = 2\pi$$

whence

$$\Phi = \frac{\bar{\Lambda}^* e^{HT}}{m} \sin 2\pi X \frac{K_0(m\alpha R)}{K_1(m\alpha)} . \tag{29}$$

Eliminating the partial derivatives of Eq. (14h) by the use of Eq. (29) yields:

$$Q_a = - \frac{We_a}{2} \frac{\rho_{air}}{\rho} \left[\frac{2\alpha}{m} \frac{K_0(\alpha m)}{K_1(\alpha m)} \bar{\Lambda} + \alpha^2 \bar{\Lambda}^{*2} e^{2HT} \sin^2 2\pi X\right] . \tag{30a}$$

Since the second term in square brackets is of order $\bar{\Lambda}^2$, it is negligible in comparison to the first. In addition, since all practical cases are those in which the jet velocity is much smaller than sonic velocity, m is taken as unity. Thus,

$$Q_a = - We_a \frac{\rho_{air}}{\rho} \frac{K_0(\alpha)}{K_1(\alpha)} \alpha \bar{\Lambda} . \tag{30b}$$

Specific Solution:

Equation (14f) is now evaluated by using Eqs. (24a), (24b), (25) and (30b)

to yield:

$$(1-\alpha^2)\bar{\Lambda} + We_a \frac{\rho_{air}}{\rho} \frac{K_0(\alpha)}{K_1(\alpha)} \alpha \bar{\Lambda} =$$

$$\left[We_a \frac{\alpha^2}{4\pi^2} \mathbf{H}^2 \frac{(1-\sigma)}{\alpha} \frac{F_0(\alpha R)}{F_1(\alpha)} \bar{\Lambda} + \frac{\alpha}{\pi} \frac{We_a}{Re_a} \mathbf{H} \left\{ (1-\sigma)\alpha \frac{F_1'(\alpha)}{F_1(\alpha)} + \sigma \alpha_1 \frac{F_1'(\alpha_1 R)}{F_1(\alpha_1)} \right\} \bar{\Lambda} \right]_{R=1} . \quad (31)$$

By virtue of Eq. (23)

$$\sigma = - \frac{4\pi\alpha}{Re_a \mathbf{H}} - \frac{2\alpha^2}{\alpha_1^2 - \alpha^2} ,$$

and the property of Bessel functions that

$$F_1'(\alpha R) = F_0(\alpha R) - \frac{1}{\alpha} F_1(\alpha R),$$

the desired relation between $\mathbf{H}$ and α is finally obtained in the following form:

$$\mathbf{H}^2 \frac{F_0(\alpha)}{\alpha^{-1} F_1(\alpha)} + \mathbf{H} \frac{4\pi}{Re_a} \alpha \left[\frac{2 F_0(\alpha)}{\alpha^{-1} F_1(\alpha)} - 1 + \frac{2\alpha^2}{\alpha_1^2 - \alpha^2} \left(\frac{F_0(\alpha)}{\alpha^{-1} F_1(\alpha)} - \frac{F_0(\alpha_1)}{\alpha_1^{-1} F_1(\alpha_1)} \right) \right] = \frac{4\pi^2}{We_a} (1-\alpha^2) + 4\pi^2 \frac{\rho_{air}}{\rho} \alpha \frac{K_0(\alpha)}{K_1(\alpha)} . \quad (32)$$

Lord Rayleigh obtained an equation similar to Eq. (32) in 1878, but it did not contain the viscosity term (in square brackets) and the aerodynamic term (second term on righthand side). In contrast to the above, his results were therefore independent of initial jet diameter and fluid properties.

First Order Solution:

For self-consistency, the functional dependences on fluid properties, diameter and velocity of Eq. (32) are reduced to linear form as it has already

been done for some of these parameters in the evaluation of the aerodynamic pressure by small perturbation theory. This is obtained by expanding some of the Bessel functions for α less than 1, namely:

$$\frac{F_0(\alpha)}{2\alpha^{-1}F_1(\alpha)} = 1 + \frac{\alpha^2}{8} - \frac{\alpha^4}{192} + \frac{\alpha^6}{3072} - \cdots \cong 1 \quad .$$

Equation (32) may be now written as:

$$H^2 + H\frac{6\pi\alpha}{Re_a} = \frac{2\pi^2}{We_a}(1-\alpha^2) + \frac{2\pi^2 \rho_{air}}{\rho}\alpha\frac{K_0(\alpha)}{K_1(\alpha)}, \qquad (33a)$$

or in dimensional form

$$\eta^2 + \frac{3\mu}{\rho a^2}\alpha^2\eta = \frac{\sigma}{2\rho a^3}(1-\alpha^2)\alpha^2 + \frac{\rho_{air}U_s^2\alpha^3}{2\rho a^2}\frac{K_0(\alpha)}{K_1(\alpha)}. \qquad (33b)$$

Due to the last term of Eq. (33), the aerodynamic term, the theory here is distinctly dependent on fluid properties and stream velocity. A typical plot of the amplification factor η vs. the wave parameter α with $U_s=0$ is shown in Fig. 6 for diethylcyclohexane and an initial jet diameter of 0.0152 cm. In this case the maximum instability occurred at $\alpha = 0.68$ or when the wave length was 4.26 times the initial jet diameter as compared to 4.51 according to the Rayleigh criterion. The validity of Fig. 6 has been demonstrated by several investigators. Donnelly and Glaberson,[20] obtained a similar result experimentally and rationalized them on the basis of the theory of Chandrasekhar, while Crane, Birch, and McCormack,[14] based their analysis on the results of Weber.

Instability Criterion:

The conditions for the uniform break up of the stream can be evaluated

by invoking Eq. (11), according to which η is required to attain a maximum. Introducing

$$B \equiv \frac{3\mu}{2\rho a^2}\ , \qquad C \equiv \frac{\sigma}{2\rho a^3}\ , \qquad D \equiv \frac{\rho_{air}}{2\rho a^2}\ , \qquad \Psi \equiv \frac{K_0(\alpha)}{K_1(\alpha)}$$

into Eq. (33b) one obtains:

$$\eta^2 + 2B\eta\alpha^2 = C(1-\alpha^2)\alpha^2 + D U_s^2 \alpha^3 \Psi$$

whence

$$\eta = -B\alpha^2 + \left[B^2\alpha^4 + C(1-\alpha^2)\alpha^2 + D U_s^2 \alpha^3 \Psi\right]^{1/2}.$$

Differentiating the above with respect to α yields,

$$\frac{\partial \eta}{\partial \alpha} = -2B\alpha + \frac{\frac{1}{2}\left[4B^2\alpha^3 + 2C(1-2\alpha^2)\alpha + 3DU_s^2\alpha^2\Psi + DU_s^2\alpha^3\Psi'\right]}{(B^2\alpha^4 + C(1-\alpha^2)\alpha^2 + DU_s^2\alpha^3\Psi)^{1/2}}$$

where

$$\Psi' \equiv \frac{d\Psi}{d\alpha}\ .$$

Since $\frac{\partial \eta}{\partial \alpha} = 0$, this may be expanded as

$$16B^2\alpha^2(B^2\alpha^4 + C(1-\alpha^2)\alpha^2 + DU_s^2\alpha^3\Psi) = 16B^4\alpha^6$$

$$+ 16B^2C(1-2\alpha^2)\alpha^4 + 24B^2DU_s^2\alpha^5\Psi + 8B^2DU_s^2\alpha^6\Psi'$$

$$+ 4C^2(1-2\alpha^2)^2\alpha^2 + 12DCU_s^2(1-2\alpha^2)\alpha^3\Psi + 4CDU_s^2(1-2\alpha^2)\alpha^4\Psi'$$

$$+ 9D^2U_s^4\alpha^4\Psi^2 + 6D^2U_s^4\Psi\Psi'\alpha^5 + D^2U_s^4\alpha^6\Psi'^2.$$

Collecting terms one obtains then:

$$U_s^4 D^2 (\alpha^6 \psi'^2 + 6\alpha^5 \psi\psi' + 9\alpha^4 \psi^2) + U_s^2 D [4C(1-2\alpha^2)(\alpha^4 \psi' + 3\alpha^3 \psi) + 8B^2\alpha^5(\psi + \alpha\psi')] + 4C^2(1-2\alpha^2)^2\alpha^2 - 16B^2C\alpha^6 = 0$$

whence

$$U_s = \left\{ - \frac{\delta + \sqrt{\delta^2 - 4\chi\beta}}{2\chi} \right\}^{1/2} \tag{34}$$

where

$$\chi \equiv D^2\alpha^4 (\alpha^2 \psi'^2 + 6\alpha\psi\psi' + 9\psi^2)$$

$$\delta \equiv 4D\alpha^3 [(1-2\alpha^2)(\alpha\psi' + 3\psi)C + 2B^2\alpha^2(\psi + \alpha\psi')]$$

$$\beta \equiv 4C^2(1-2\alpha^2)^2\alpha^2 - 16B^2C\alpha^6 .$$

Since α is related to the frequency of the drop formation, selection of a critical frequency in Eq. (34) will determine the corresponding initial jet velocity.

EXPERIMENTAL RESULTS OF MECHANICAL GENERATION OF DROPS

Uniform drops were produced using method (d) of Fig. 1 with the voice coil of a loud speaker acting as the vibrator for the membrane. Results were obtained for small thin tubes of gauges 30, 27, and 24 (ie. internal diameter of 0.0152, 0.0200, and 0.0290 cm respectively), and three fluids; diethylcyclohexane (DECH), iso-octane, and normal heptane. Properties of these fluids are listed in Table I. Because of the frequency limitations of the voice coil, only vibrations of up to 12kc could be produced with sufficient energy to cause a varicose stream as illustrated in Figs. 2a and 3b.

From the solution, Eq. (33a), it appears that the problem is governed essentially by four non-dimensional parameters, Re, We, $\frac{\rho_{air}}{\rho}$ and α. The latter is directly related to the well known Strouhal number, since:

$$St \equiv \frac{2fa}{U_s} = \frac{\alpha}{\pi} . \tag{35}$$

Consequently, it is most proper to seek a correlation of the results in the following form:

$$St = K Re^{\gamma} Z^{\beta} \left(\frac{\rho_{air}}{\rho} \right)^{\omega} \tag{36}$$

where K, γ, β and ω are constants to be determined from experimental results, and

$$Z = \frac{\mu}{(\rho \sigma d)^{1/2}} = \frac{We^{1/2}}{Re}$$

is the Ohnesorge number where the Weber and Reynolds numbers are based on the initial jet diameter.

The dimensional correlation above was based on the concept that the basic equations contained, at least, all of the pertinent parameters. Experimental results indicate, however, no noticeable dependence on the ratio, $\frac{\rho_{air}}{\rho}$, that appears in Eq. (36). On the other hand a pronounced influence of the ratio of viscous and surface tension forces in the form

$$\Gamma \equiv \frac{\mu C}{\sigma}$$

(C expressing the velocity of sound in the liquid) has been noted. Instead of Eq. (36), experimental results correlate better according to the following relationship:

$$St = K Re^{\gamma} Z^{\beta} \Gamma^{\omega} . \tag{37}$$

Since C was nearly constant for the fluids tested, Γ was in effect just a measure of the variation of μ/σ.

Figure 7 illustrates typical St-Re results for DECH and tubes of #27 gauge. The band of Strouhal number for each Reynolds Number does not reflect the accuracy of the experiment but the range of frequencies over which a uniform stream of drops could be generated at a given flow rate. Whereas according to Eq. (11) the condition for the jet to disintegrate into uniform drops was $\frac{\partial \eta}{\partial \alpha} = 0$, from Fig. 6 it appears that there is a range of α (and hence a range of Strouhal number) over which $\frac{\partial \eta}{\partial \alpha}$ is almost zero. It should be noted that the frequency upon which the Strouhal number is based was not the frequency at which the diaphragm of the spray head vibrated (see Fig. 4), but rather the value obtained by dividing the volumetric flow rate of the stream by the drop volume. The difference between this frequency and the input frequency was a characteristic of the geometry of the drop generator and fluid properties.

While uniform drops were generated over a range of frequencies at each Reynolds number, the generated flow was not the same for each frequency and thus some subjective selection had to be made on the extent of the range. Figure 8a, 8b, 8c shows DECH drops emitted at the same Reynolds number (428) from a #27 gauge tube at drop frequencies of about 2.9, 4.1 and 4.5 kc. Notice that while the drops were uniform, they were not uniformly spaced, because each one traveled in the wake of preceding drops and thus experienced different amounts of drag. Obviously, at the same flow rate an increase in frequency would increase the number of drops generated and this would, in turn, reduce their volume (here drop sizes ranged from 400 to 340 microns). In Fig. 8c, however, the drops were generated close enough together so that variations in spacing caused some drops to coalesce.

While it was implied in the theory and dimensional analysis that the L/d of the tube generating the liquid filament did not affect the basic characteristics of the problem, Fig. 7 gives some evidence of such effects. One may presuppose that when $L/d = 33.3$, it was too small to produce a

sufficiently straight and parallel flow in order to yield a consistent response on the Re-St plane. On the other hand, when $L/d = 100$, it might have been too large so that the pressure waves induced by the vibrator were damped down to negligible intensity after encountering greater viscosity losses in the longer tube, thus limiting the attainable performance to $Re \leqslant 900$.

Constants K, δ, β and ω were found by drawing best lines through data similar to Fig. 7 and correlating them according to Eq. (37). They are tabulated in Table II for the fluids described in Table I. Since, for values of $Re \leq 1800$, the exponents of Z and Γ were constant, all experimental results in this range of Reynolds number can be correlated in terms of

$$St\, Z^{1/2}\, \Gamma^{-2/3} = f(Re)$$

as shown in Fig. 9.

Figure 9 demonstrates the existence of three flow regimes, while only one (i.e. regime II) was predicted from the theory. No specific curves were defined in regime III since the flow exiting the tube was often atomized before varicosity could be established, and results were partly dependent on the L/d of the tube. Regime I extended from where the flow from the tube first becomes a filament rather than a series of drips. For a single flow rate near this transition point for each tube, the resultant drops were uniform without the addition of outside periodic forces. When the filament surface was vibrated at a frequency less than that at which the drops formed naturally, the uniformity was destroyed, while any higher frequency had no effect on the drops.

The deviation from the theory in regimes I and III could be attributed to the fact that the analysis has been based on the assumption of negligible convective acceleration in comparison to local acceleration. This clearly fails when velocity gradients become sufficiently large due to turbulence (as in regime III) or gravity (as in regime I). An approximate drag calcula-

tion on a filament in regime I shows that it would reach its terminal velocity at a stream Reynolds number of about 500.

In the St-Re plane of Fig. 10, the "best fit" of experimental results is compared with the theoretical solution of Eq. (34) for DECH. While the theory did appear to have a proper functional dependence on Reynolds number, it did not bring out a significant effect on initial jet diameter. However, for each fluid, the use of $Z^{0.5}$, which is independent of stream velocity, correlated experimental results into a form independent of diameter. Thus, although the theory did not properly take into account the diameter dependence, in practice this can be eliminated from the problem by the empirical correlation. It should be noted, however, that for Reynolds numbers larger than 400, the theory predicts an incorrect trend for the dependence on the initial jet diameter, and this may be attributed to neglecting the second term in Eq. (30a). The effect of this was the reduction of the solution of the aerodynamic pressure, Q_a, to that of the plane problem rather than the axisymmetric one. This should have a significant effect in the case of smaller tube diameters.

For the interest of spray combustion, the most important results were not merely uniformity of the drops but also drops sizes obtainable. These results are illustrated by Fig. 11 for DECH. Again, the range of drop sizes for each Re reflected the fact that a range of frequencies produced uniform drops. For example after Re = 600 - 700 the drop diameters obtainable were quite constant and about 1.8 tube diameters.

Using the 1.8 rule, it is possible to get a feel for the drop size capabilities of the capillary instability method used here. Figure 12 is a performance map constructed in this manner for DECH. It illustrates clearly that the practical limit of sonic vibrations ($\sim$16kc) is 200 micron diameter drops in DECH. Since the 1.8 law is only valid for Reynolds number over 600, even if a high frequency vibrational device could be employed to produce drops of an order of 50 microns, the rather formidable problem of generating a laminar flow of about Re = 600 in a 28 micron diameter tube may render it quite impractical. Figure 12 also illustrates that the requirement for drops with

diameters of less than 200 microns leads to ultrasonic drop generation. This is the subject of the next section.

ULTRASONIC DROP GENERATION

Small droplets of the range of 20 to 200 microns could have been generated by tearing them off two charged surfaces with electrostatic potential, [21, 22] by growing them with submicron neuclation particles in a "rain chamber", or by selecting satellites (shown in Fig. 3a) by periodic electrostatic forces. However, the most practical method employed ultrasinic vibrations produced by a piezoelectric crystal.

As a direct extension of the method presented above, small holes could be drilled in the crystal and fluid forced through them as the crystal vibrated at the critical frequencies. Combs [23] and his associates have been able to establish 150 and 200 micron water drops using this method.

It was also possible to replace the vibrating membrane of Fig. 4 by submersing an electrically excited crystal in the fluid chamber. In this configuration, a plate containing the thin tubes and a dummy plate were placed at 1/4 of a wave length of the excited frequency on either side of the crystal. Thus establishing standing pressure waves in the fluid. However, because of viscosity losses in the fluid chamber and a mismatch of acoustic velocity in the crystal and fluid, pressure waves of sufficient magnitude to produce a varicose stream could not be established.

A design developed by the J.D. Little Company for the American Petroleum Institute operates on a similar principle as the above but without its drawbacks. The phenomenological aspects of the generator shown in Fig. 13 have been fully described in API Proceedings over the last several years [24, 25, 26]. The signal generator and amplifier excite the crystal at a fixed frequency. Acoustic waves propagate into the two horns, which are made of material with the same acoustic velocity as the crystal, (i.e. aluminum) and which were 3/4 of a wave length long. A standing wave is thus generated in the horns with the fluid to be atomized slurred on the face of one vibrating

horn. The particle field generated by this atomizer is shown in Fig. 14 for a flow rate of approximately 0.50 ml/sec. While the droplets shown are not of uniform size, the predominant size is 50 microns and is considerably more uniform than other methods investigated in this size range.

SUMMARY AND CONCLUSIONS

A theory was presented to determine critical frequencies of a liquid filament as a function of fluid viscosity surface tension and density as well as initial jet diameter and velocity. Both theoretical and experimental results were applicable to methods of generating uniform drops which utilized capillary instability. Experimental results indicated that for a fixed set of jet and fluid properties, there was a spread of critical frequencies which generated uniform drops, rather than a unique frequency as predicted from theory. While the theory did predict a proper functional dependence on Reynolds number for a filament no longer governed by gravitational effects ($Re > 500$) but not yet turbulent ($Re < 2000$), it did not bring out a significant dependence of initial jet diameter. Experimental results for a given fluid, however, were also rendered independent of initial jet diameter by use of the square root of the Ohnesorge number.

It was found that the smallest drop sizes capable of being produced by capillary instability were 1.8 times initial jet diameters, and thus the practical limit of this method without resulting to ultrasonics would be 200 micron drops. The ultrasonic devices investigated thus far have not generated a sufficiently uniform flow field for combustion experiments, although they are well capable of producing drops of 10 to 50 microns.

REFERENCES

1. Busch, C. W., Laderman, A. J., Oppenheim, A. K., "Generation of Flow Fields in Particle Fueled Combustion Systems", SSL Tech. Note #1, NASA Grant NsG-702, Series 6, Issue 17, University of California, Berkeley, May, 1965.

2. Burgoyne, J. H. and Cohen, L., "The Effect of Drop Size on Flame Propagation in Liquid Aerosols", Proc. Roy. Soc., A225, pp. 375-392.

3. Hartmann, J., The Plate-Jet, Danmarks Naturvidenskabelige Samfrust, Kobenhavn, 1935.

4. Vonnegut, B., Neubauer, R. L., "Production of Monodisperse Liquid Particles by Electrical Atomization", J. Colloid Sci., F(6), pp. 616-622, 1952.

5. Rayner, A. C., Hurtig, H., "Apparatus for Producing Drops of Uniform Size", Science, p. 672, October 22, 1954.

6. Miesse, C. C., "The Effect of Ambient Pressure Oscillations on the Disintegration and Dispersion of a Liquid Jet", Jet Propulsion, 25, pp. 525, October 1955.

7. Rayner, A. C., Haliburton, W., "Rotary Device for Producing a Stream of Uniform Drops", Rev. of Sci. Inst., 26, pp. 1124-1127, 1955.

8. Magarvey, R. H., Taylor, B. W., "Apparatus for the Production of Large Water Drops", Rev. of Sci. Inst., 27, pp. 944-947, 1956.

9. Wolf, W. R., "Study of the Vibrating Reed in the Production of Small Droplets and Solid Particles of Uniform Size", Rev. of Sci. Inst., 32, pp. 1124-1129, 1961.

10. Mason, B. J., Jayaratne, O. W., Woods, J. B., "An Improved Vibrating Capillary Device for Producing Uniform Water Droplets of 15 to 500 μ Radius", J. Sci. Inst., 60, pp. 247-249, 1963.

11. Mason, B. J., Brownscombe, J. L., "Production of Uniform Size Drops at Controllable Frequency and Spacing from a Vibrating Capillary", J. Sci. Inst., 41, pp. 258, 1964.

12. Schneider, J. M., Hendrichs, C. D., "Source of Uniform-Sized Liquid Droplets", Rev. of Sci. Inst., 35, pp. 1349-1350.

13. Ryley, D. J., Wood, M. R., "The Construction on Operating Characteristics of a New Vibrating Capillary Atomizer", J. Sci. Inst., 40, pp. 303-305, 1963.

14. Crane, L., Birch, S., McCormack, P. D., "The Effect of Mechanical Vibration on the Break-Up of a Cylindrical Water Jet in Air", Brit. J. Appl. Phys., 15, pp. 743-750, 1964.

15. McCormack, P. D., Crane, L., Birch, S., "An Experimental and Theoretical Analysis of Cylindrical Liquid Jets Subjected to Vibration", Brit. J. Appl. Phys., 16, 1965.

16. Rayleigh, J. W. S., The Theory of Sound, Dover Publications, Inc., New York, First Edition, 1877.

17. Rayleigh, J. W. S., "On the Instability of Jets", Proc. London Math Soc., 10, pp. 4, 1878.

18. Weber, C., "Zum Zerfall eines Flursigkeitsstrahiles", Z. angew. Math. Mech., 11, pp. 136-154, 1931.

19. Chandrasekhar, S., Hydrodynamic and Hydromagnetic Stability, pp. 515-576, Clarendon Press, Oxford, 1961.

20. Donnelly, Glaberson, "Experiments on the Capillary Instability of a Liquid Jet", Proc. of the Roy. Soc., Series A, p. 547, March 5, 1966.

21. Luther, F. E., "Electrostatic Atomization of No. 2 Heating Oil", Proc: API Research Conference, API Publication 1701, June 19, 1962.

22. Peskin, R. L., Raco, R., Yeh, P.S., Morehouse, J., "A Study of the Parameters Governing Electrostatic Atomization of Fuel Oil", Proc: API Research Conference, API Publication 1704, June 1, 1965.

23. Combs, P., Manson, L., Rocketdyne Division of North American Aviation, Private Communications.

24. Doyle, A. W., Mokler, B. V., Perron, R. R., "New Means of Fuel Atomization", Proc: API Research Conference, API Publication 1701, June 19, 1962.

25. O'C. Young, J. C., Wilson, J. A., Lang, R. J., "An Ultrasonic Oil Burner", Proc.: API Research Conference, API Publication 1701, June 19, 1962.

26. McCullough, J. E., Perron, R. R., Shanley, E. S., "The API Ultrasonic Atomizer and Oil Burner Program", Proc: API Research Conference, API Publication 1704, June 1, 1965.

TABLE I

FLUID PROPERTIES

	Density g/cc	Surface Tension Dyne/cm	Viscosity Centipoise	Sound Speed cm/sec*
DECH	.8000	27.00	1.14	1.23×10^5
Iso-Octane	.6963	18.77	0.503	1.16×10^5
N-Heptane	.6882	20.14	0.417	1.13×10^5

* Estimated Valves

TABLE II

DIMENSIONAL ANALYSIS RESULTS

Re	K	δ	β	ω
500	1.3×10^{-5}	0.8	- 1/2	2/3
500-1800	1.5×10^{-3}	0.07	- 1/2	2/3
1800	-	-	-	-

Where $St = K Re^{\delta} Z^{\beta} \Gamma^{\omega}$

FIGURE CAPTIONS

Fig. 1 Methods for Mechanical Generation of Uniform Drops

Fig. 2 Type of Streams Produced. Fig. 2a was produced using method c of Fig. 1, while 2b was produced using method d.

Fig. 3 Occurrence of Saellite Drops

Fig. 4 Spray Head Used in Combustion Experiments

Fig. 5 Configuration of Liquid Filaments Produced by Periodic Vibrations

Fig. 6 Amplification Factor vs. Wave Number for DECH and a #30 Gauge Tube

Fig. 7 The L/d Effect on the St-Re Plane. For DECH and a #27 Gauge Tube

Fig. 8 Drop Variations at a Fixed Reynolds Number. Re = 428, drop frequencies of 2890, 4080 and 4550 cps respectively.

Fig. 9 Results of Dimensional Analysis

Fig. 10 Comparison of Theoretical (Bottom) and Experimental (Top) Results for DECH

Fig. 11 Drop Diameters Obtainable with DECH

Fig. 12 Drop Size Performance Map for DECH

Fig. 13 API Ultrasonic Atomizer

Fig. 14 Spray Field Generated with Ultrasonic Atomizer

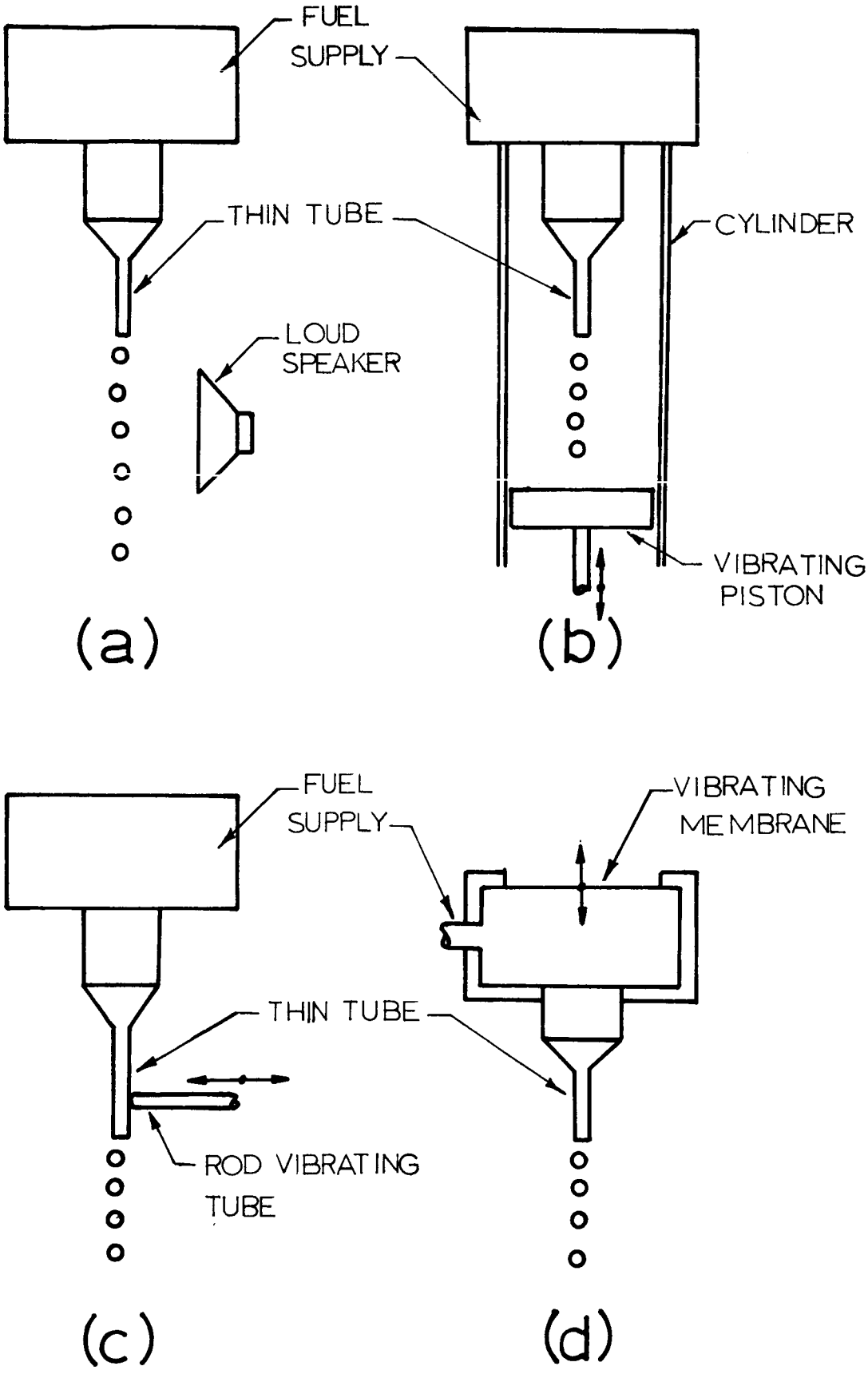
FUEL
SUPPLY
THIN TUBE
LOUD
SPEAKER
(a)
CYLINDER
VIBRATING
PISTON
(b)
FUEL
SUPPLY
VIBRATING
MEMBRANE
THIN TUBE
ROD VIBRATING
TUBE
(c)
(d)

FIG. 1

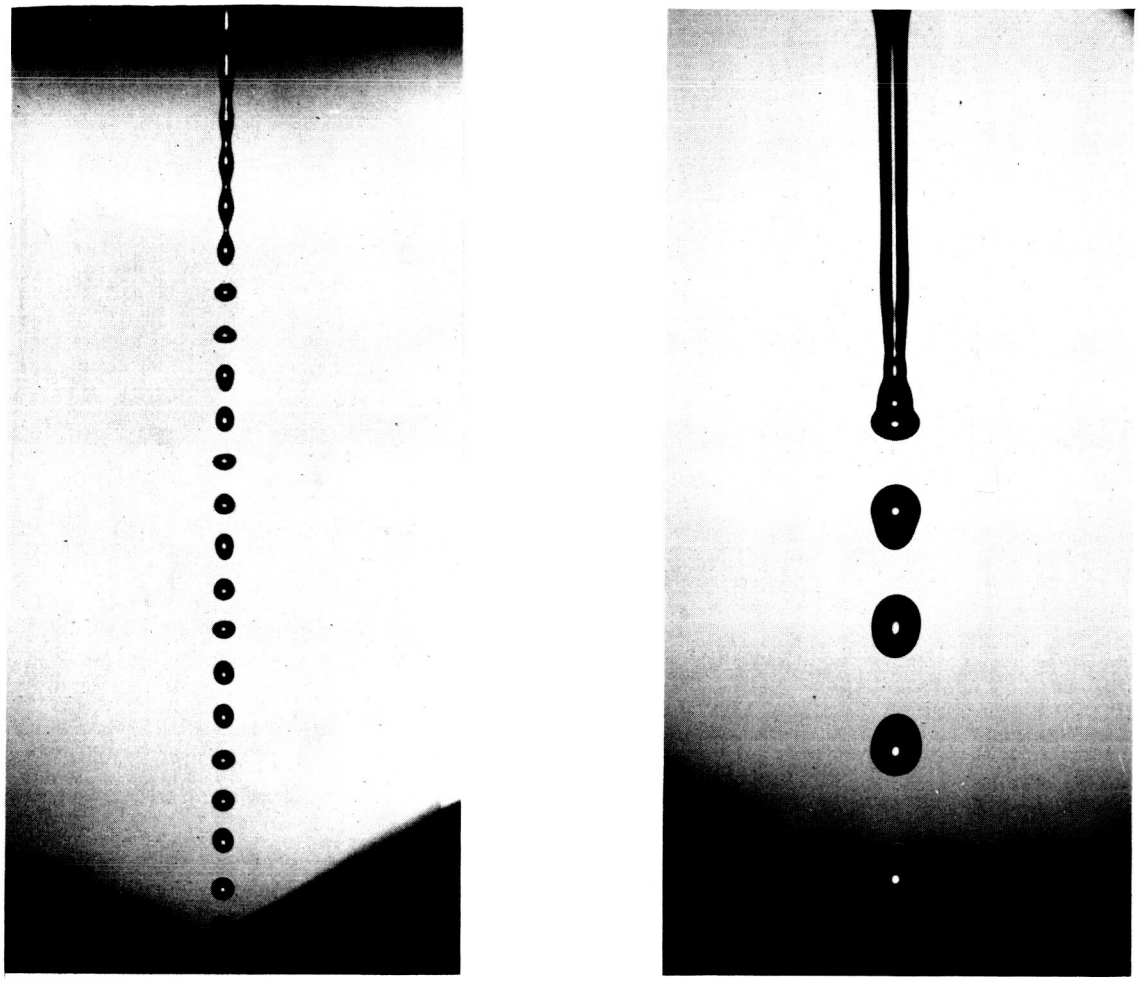

(a) (b)

FIG. 2

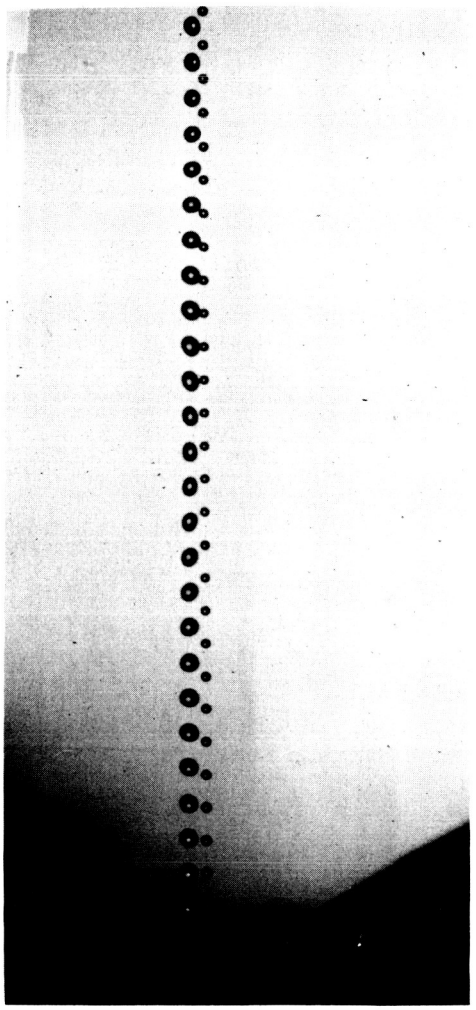

(a)

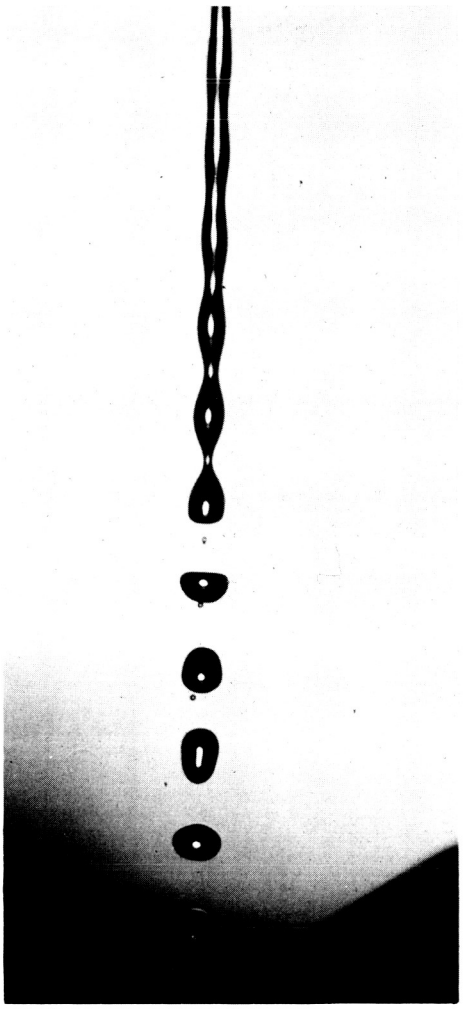

(b)

FIG. 3

SPRAY HEAD

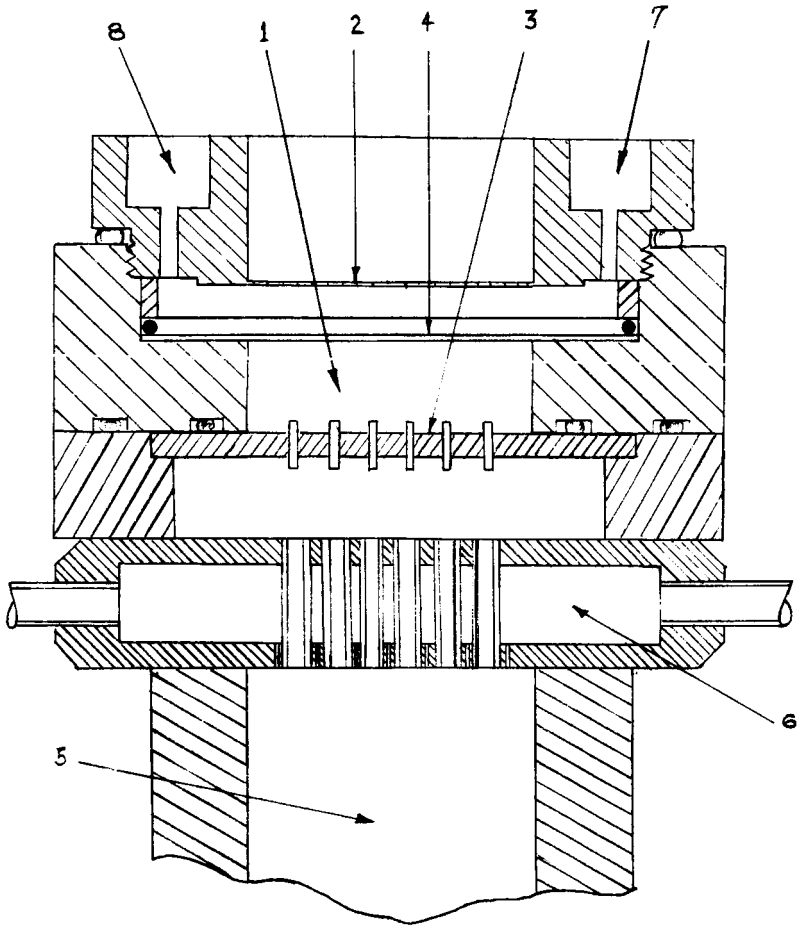

1. FUEL CHAMBER
2. DIAPHRAGM
3. PLATE
4. FILTER
5. REACTION TUBE
6. O_2 AND N_2 CHAMBER
7. VENT
8. FUEL SUPPLY

FIG. 4

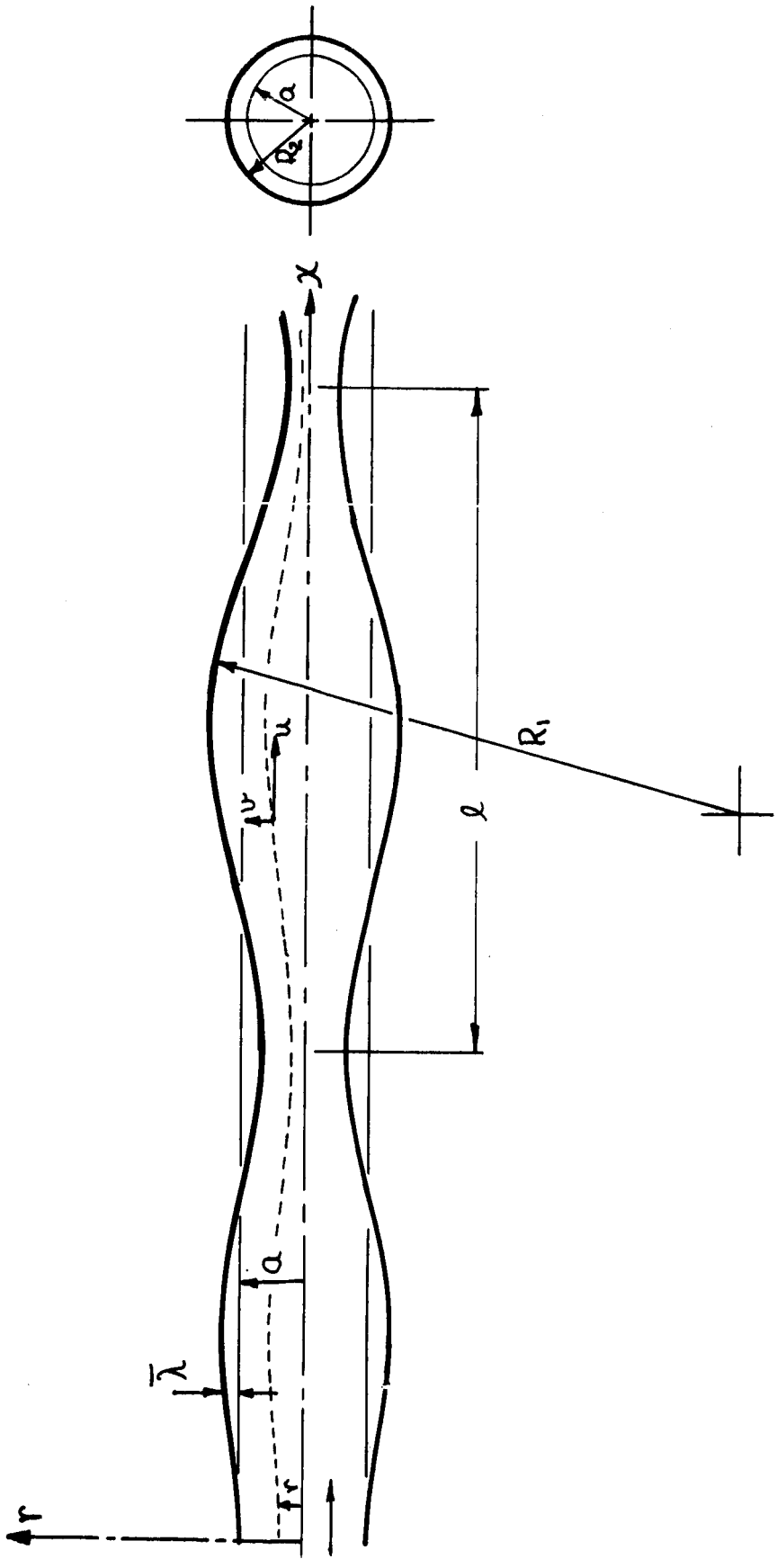

FIG. 5

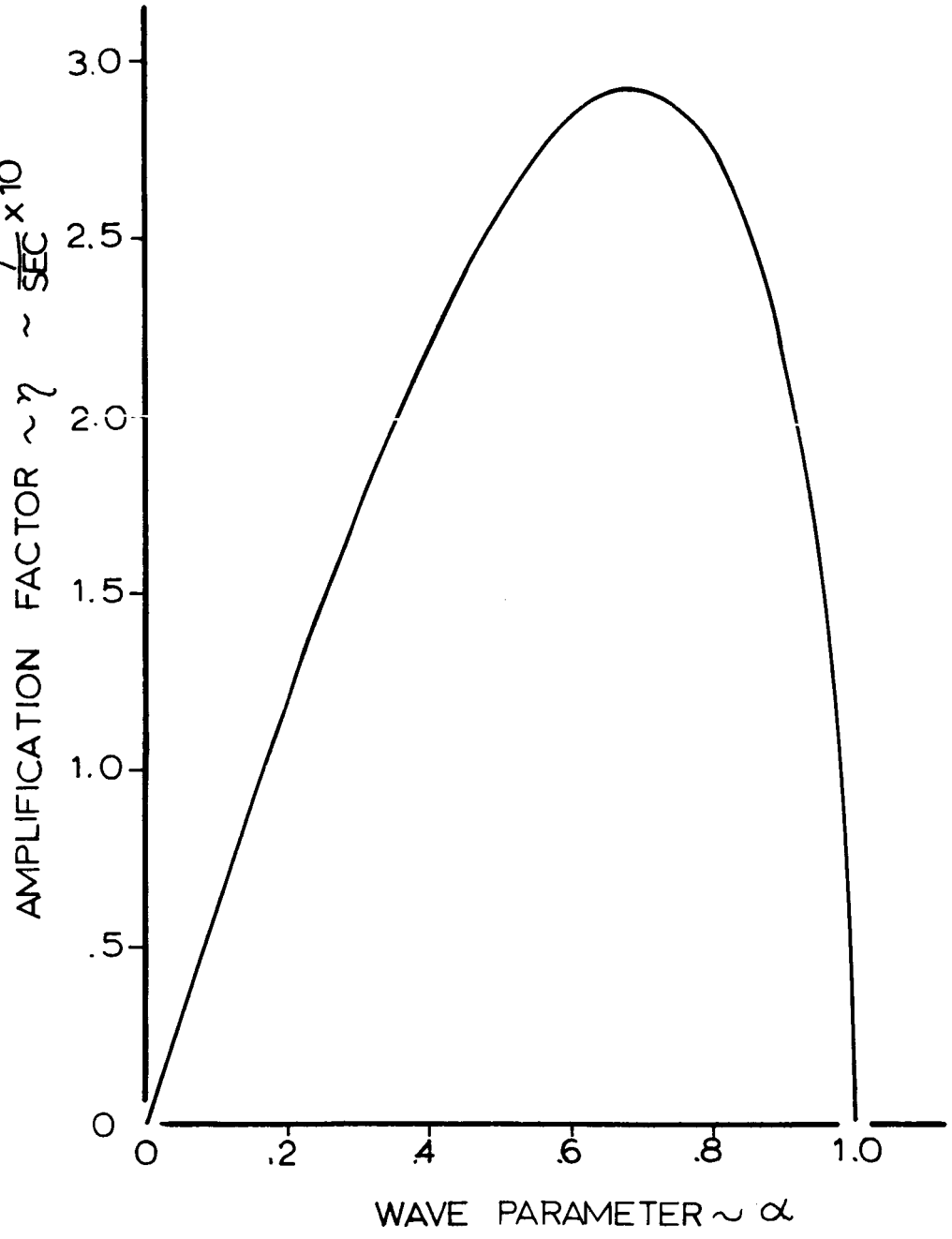
AMPLIFICATION FACTOR ~ η ~ 1/SEC x 10^3
3.0
2.5
2.0
1.5
1.0
.5
0
0
.2
.4
.6
.8
1.0
WAVE PARAMETER ~ α

FIG. 6

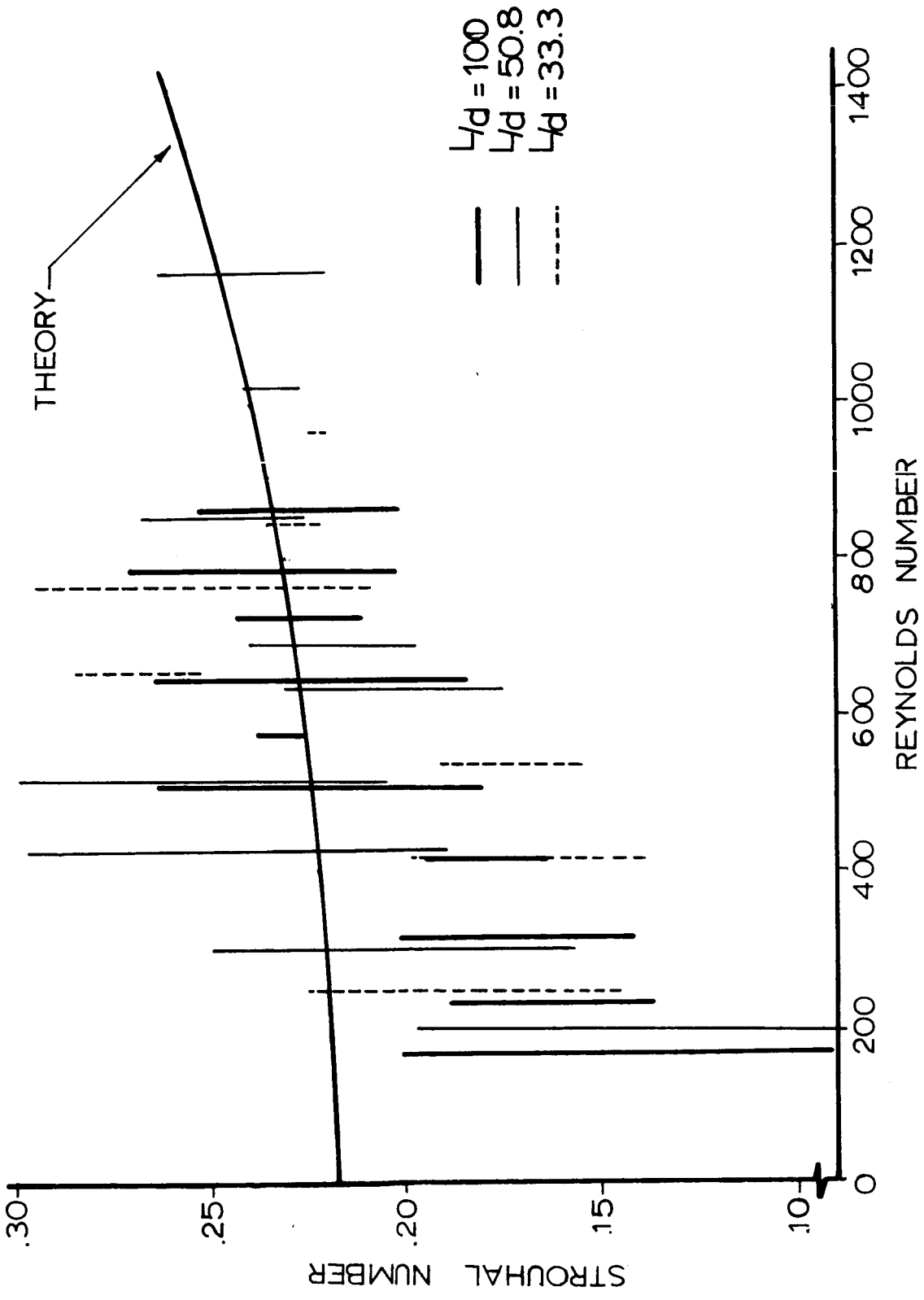
THEORY
L/d = 100
L/d = 50.8
L/d = 33.3
STROUHAL NUMBER
.30
.25
.20
.15
.10
0
200
400
600
800
1000
1200
1400
REYNOLDS NUMBER

FIG. 7

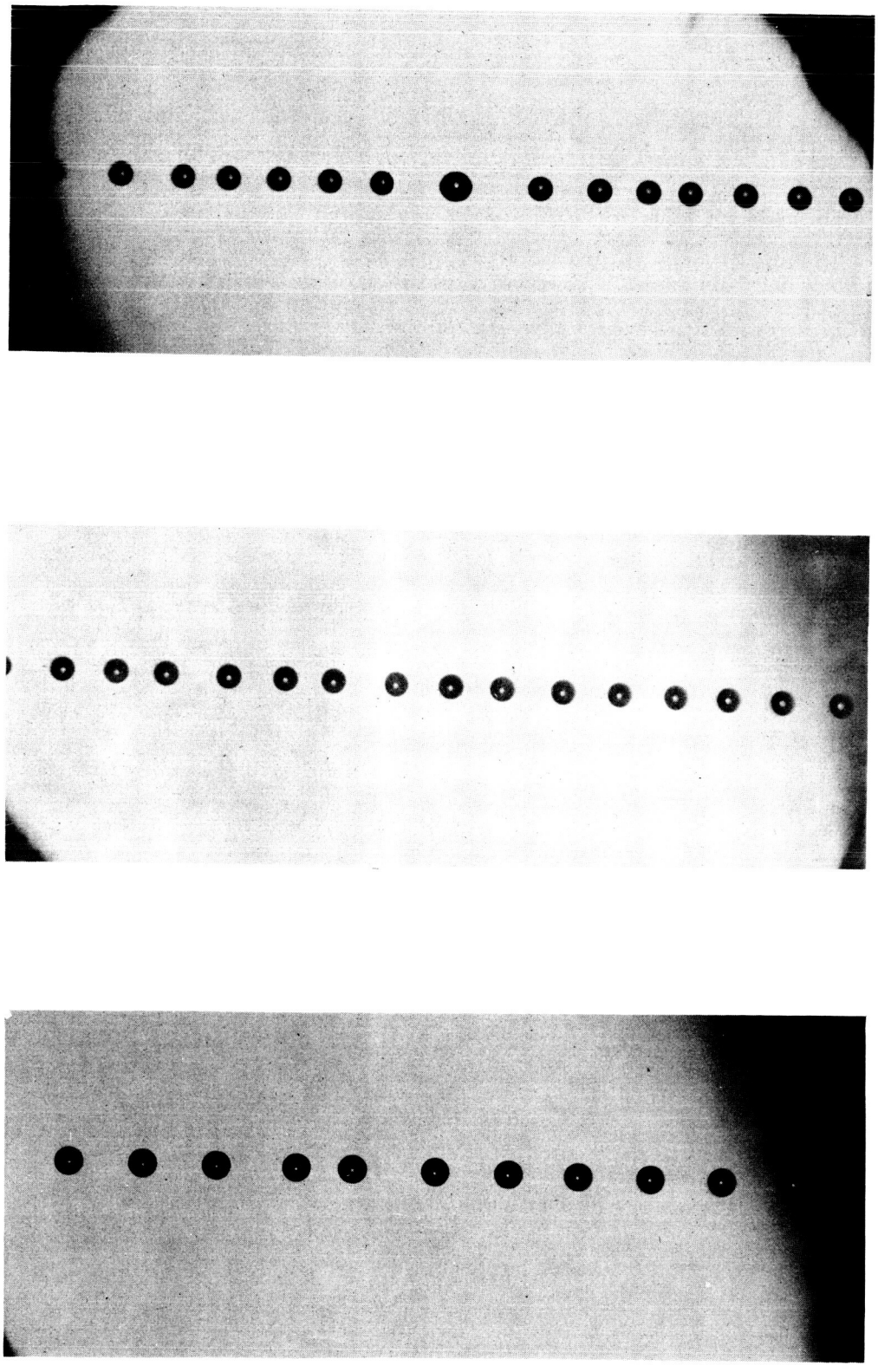

FIG. 8

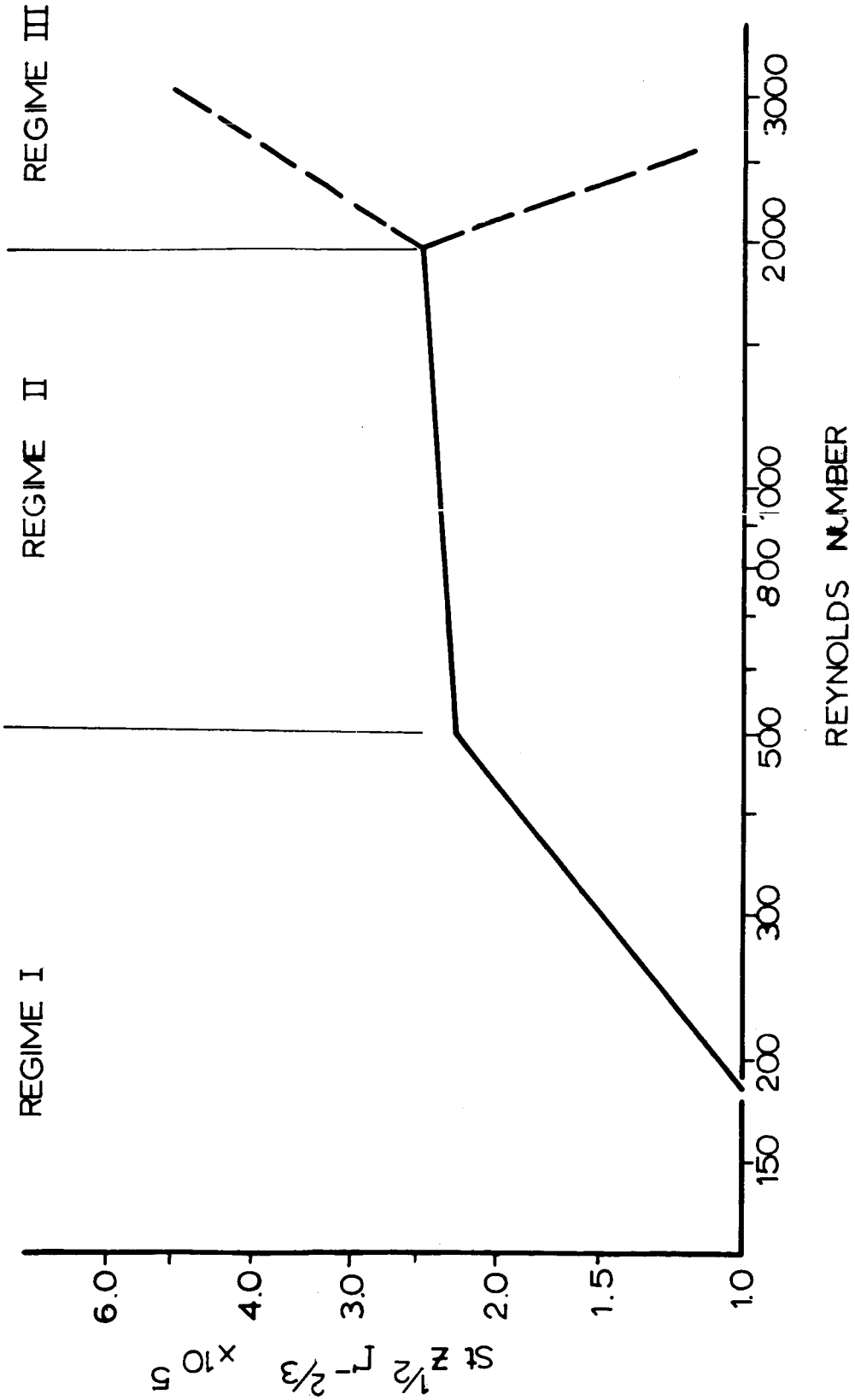
REGIME I
REGIME II
REGIME III
REYNOLDS NUMBER
150
200
300
500
800
1000
2000
3000
1.0
1.5
2.0
3.0
4.0
6.0
St Z^1/2 Γ^-2/3 x10^5

FIG. 9

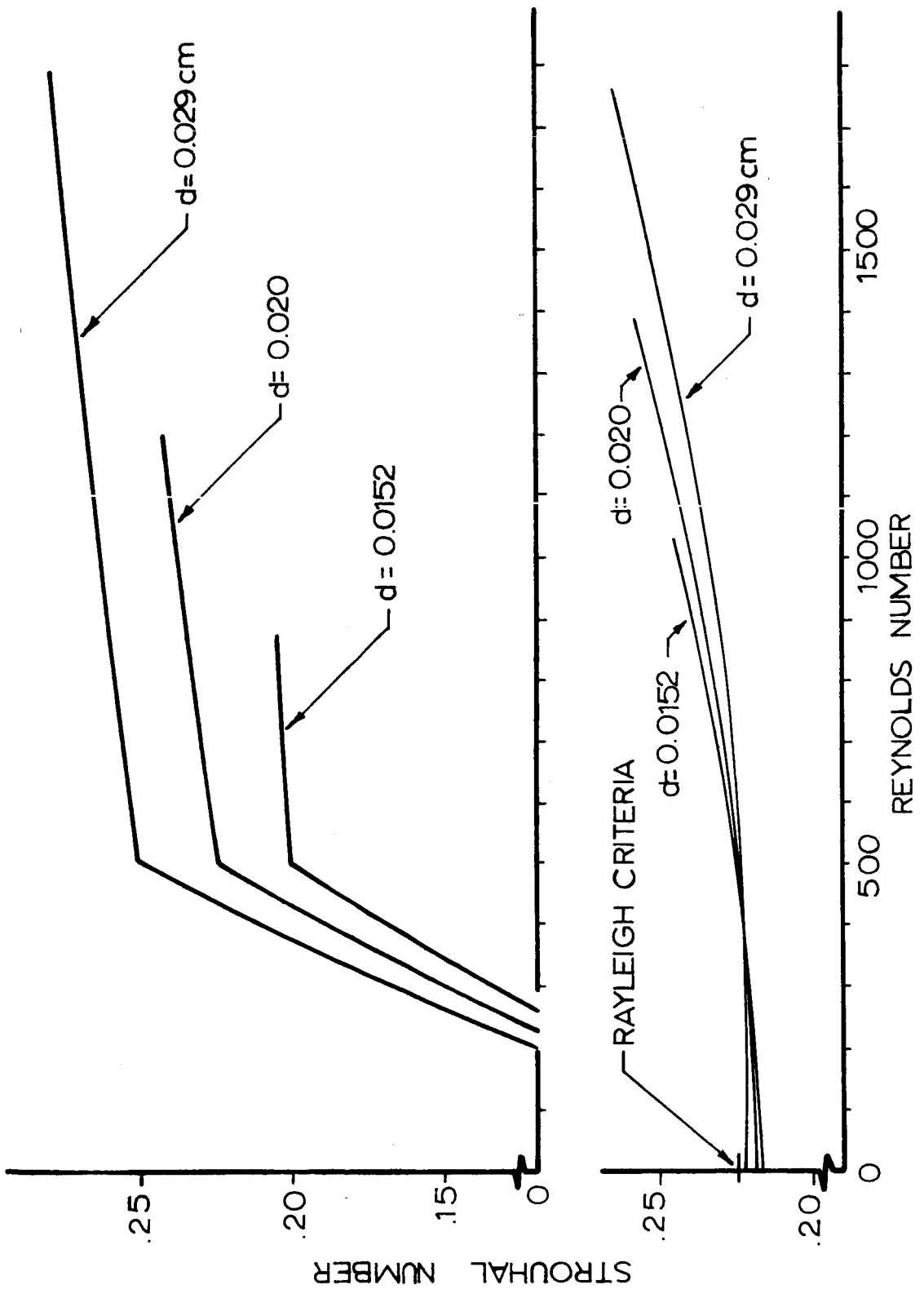
STROUHAL NUMBER
.25
.20
.15
0
d=0.029 cm
d= 0.020
d = 0.0152
RAYLEIGH CRITERIA
d= 0.0152
d= 0.020
d=0.029 cm
500
1000
1500
REYNOLDS NUMBER

FIG. 10

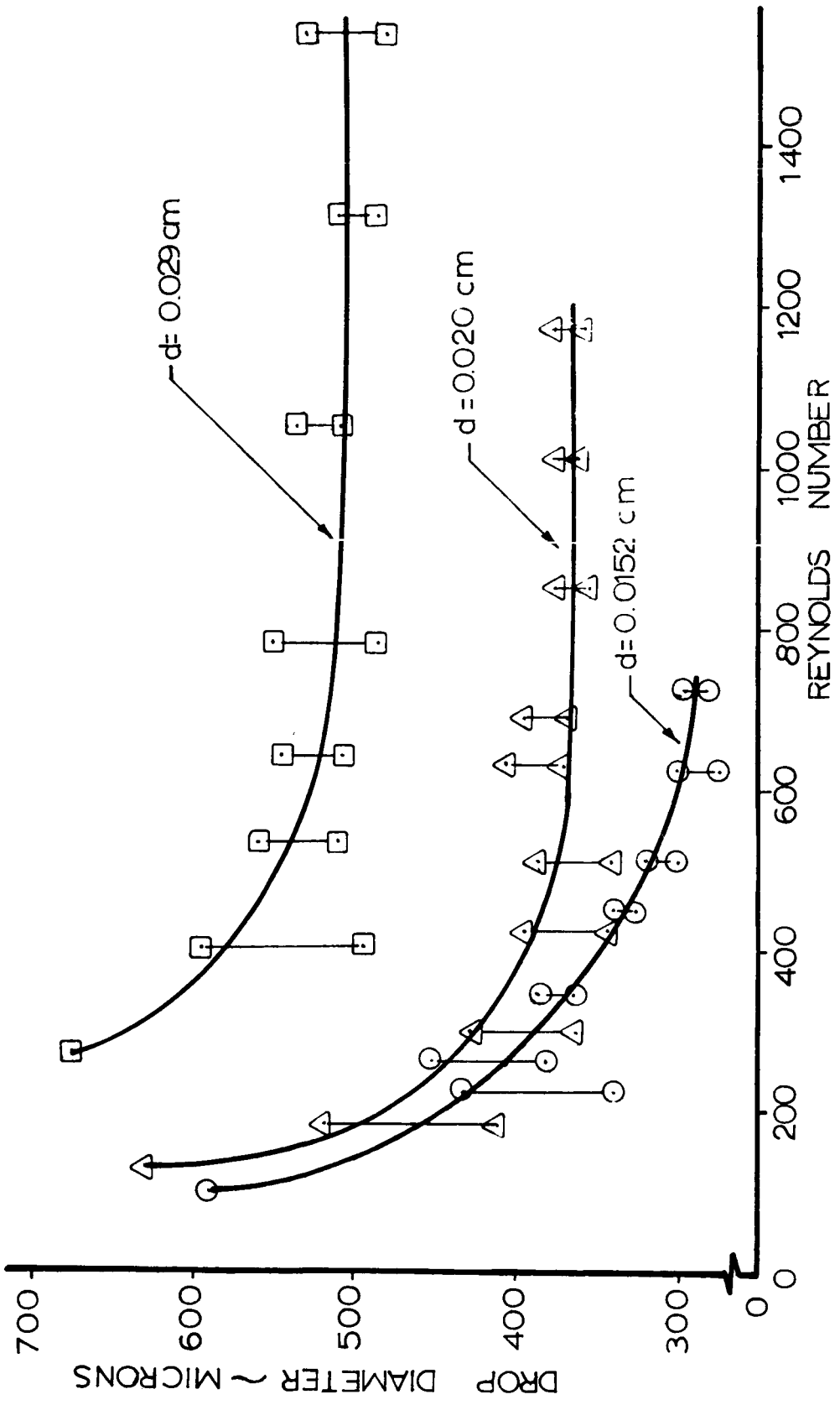
d= 0.029 cm
d = 0.020 cm
d= 0.0152 cm
DROP DIAMETER ~ MICRONS
700
600
500
400
300
0
200
400
600
800
1000
1200
1400
REYNOLDS NUMBER

FIG. 11

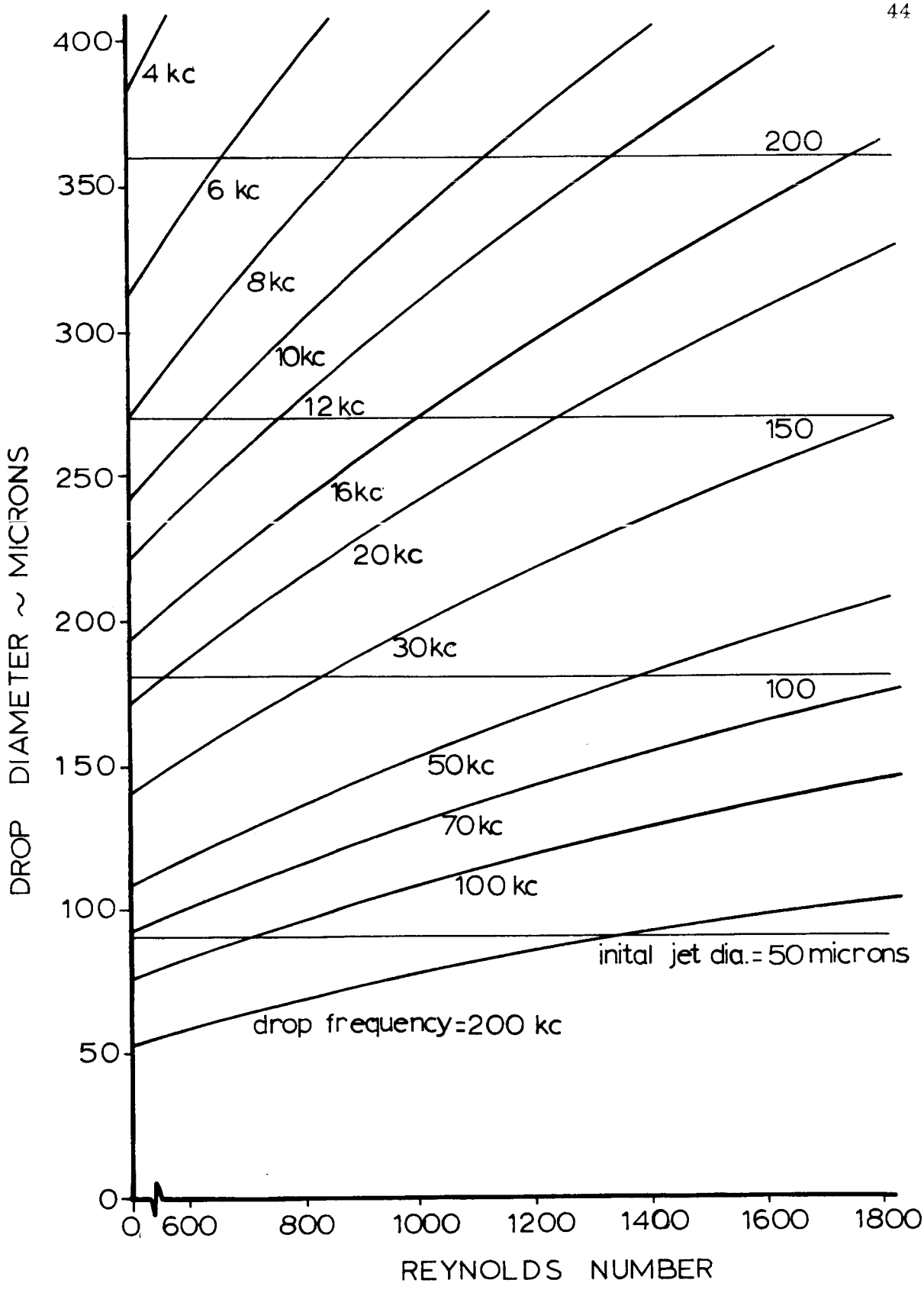
400
350
300
250
200
150
100
50
0
DROP DIAMETER ~ MICRONS
4 kc
6 kc
8kc
10kc
12 kc
16kc
20kc
30kc
50kc
70kc
100 kc
200
150
100
inital jet dia.= 50 microns
drop frequency=200 kc
0
600
800
1000
1200
1400
1600
1800
REYNOLDS NUMBER

FIG.12

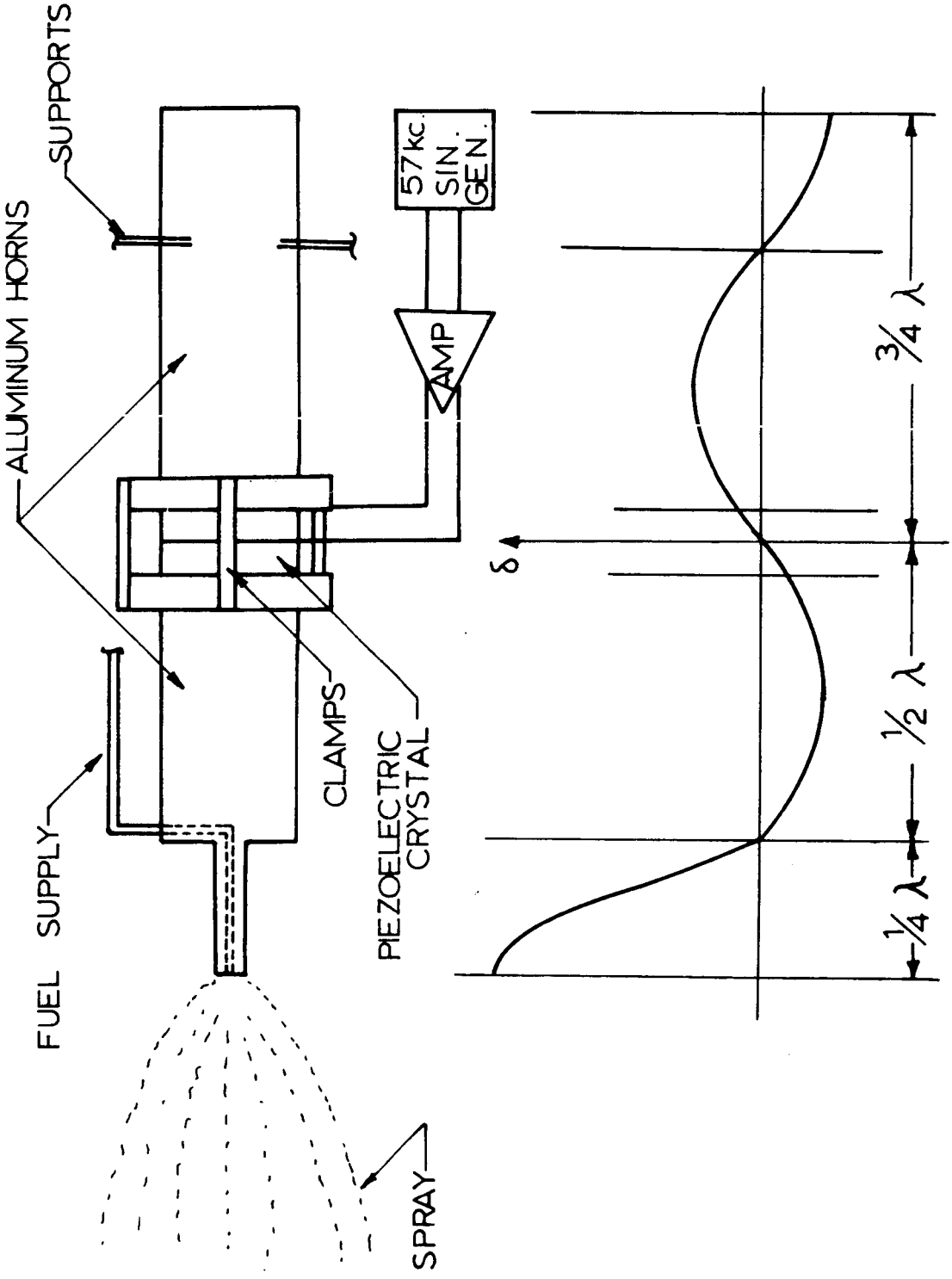
SUPPORTS
ALUMINUM HORNS
57 kc. SIN. GEN.
AMP
FUEL SUPPLY
CLAMPS
PIEZOELECTRIC CRYSTAL
SPRAY
δ
¾ λ
½ λ
¼ λ

FIG. 13

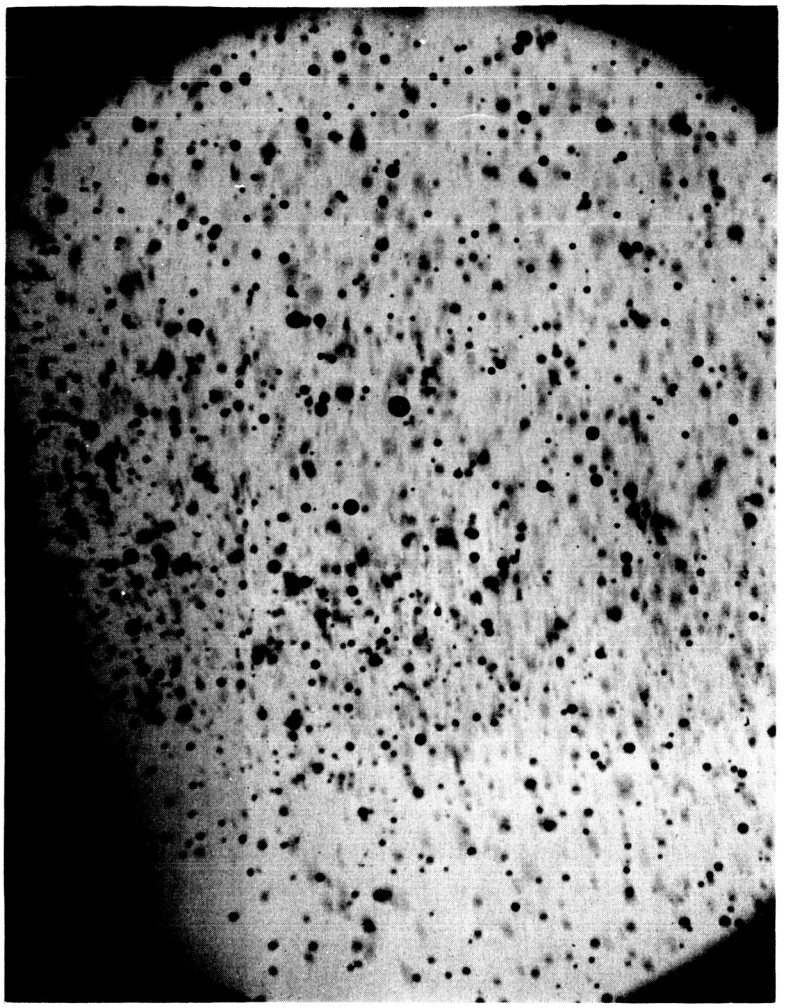

FIG. 14